

# Flight Investigation of Gyroplane Longitudinal Flight Dynamics

Dr. Stewart S. Houston  
Dr. Douglas G. Thomson

Dept. of Aerospace Engineering  
University of Glasgow  
Glasgow  
Scotland  
G12 8QQ

## Abstract

This Paper presents an analysis of test data recorded during flight trials of a gyroplane. This class of rotary-wing aircraft has found limited application in areas other than sport or recreational flying. However, the accident rate is such that a study of the configuration's stability and control characteristics is timely, and in addition substantive data is required for a new airworthiness and design standard that is under development. The Paper presents a unique coupling of established parameter estimation techniques with data from a class of aircraft that has received no attention in the contemporary literature. As a consequence, the Paper helps to consolidate the status of system identification as a powerful tool in the analysis of rotorcraft engineering problems. It is concluded that robust estimates of the longitudinal stability and control derivatives have been identified, indicating benign and "classical" longitudinal stability and control characteristics. However, unlike most helicopters, the rotorspeed degree of freedom must be included in the model structure.

## Nomenclature

$A, B$	state-space system and control matrices	$\alpha_{vane}, \beta_{vane}$	angle of attack and sideslip measured at vane location, rad
$i$	imaginary operator	$\Delta f$	frequency increment, rad/s
$M_u, M_w, etc$	pitching moment derivatives, 1/(ms)	$\Delta t$	time increment, s
$p, q, r$	angular velocity components about body axes, rad/s	$\eta_s$	longitudinal stick position, % (0% fully forward)
$Q_u, Q_w, etc$	rotor torque derivatives, rev/min/(m)	$\Omega$	rotorspeed, rev/min
$Re[], Im[]$	real and imaginary components of []	$\omega$	frequency, rad/s
$R$	regression correlation coefficient		
$T, T_p$	rotor, propeller thrust, N		
$T(u, w)$	rotor thrust in $(u, w)$ disturbed flight, N		
$u, w$	velocity components along longitudinal, vertical body axes, m/s		
$X_u, X_w, etc$	longitudinal body axis acceleration derivatives, 1/s		
$\underline{x}, \underline{u}$	state and control vectors		
$\underline{x}(\omega), \underline{u}(\omega)$	Fourier-transformed state and control vectors		
$u_{probe}, w_{probe}$	velocity components along longitudinal, vertical air data probe axes, m/s		
$x_{vane}, y_{vane}, z_{vane}$	angle of attack and sideslip vane location in body axes, m		
$x_{cg}, y_{cg}, z_{cg}$	aircraft centre-of-mass position in body axes, m		
$Z_u, Z_w, etc$	vertical body axis acceleration derivatives, 1/s		

## Introduction

There are a wide range of configurations in the class of aircraft known as rotorcraft. The helicopter is the most common type, finding widespread application in commercial and military aviation. The gyroplane (or gyroplane), however, is an increasingly popular machine in sport and recreational flying, having found no practical application in contemporary commercial or military roles.

Currently, most if not all types of gyroplane are in the homebuilt, or experimental category. The study of the configuration's flight mechanics is timely, given the accident rate suffered by the aircraft. For example, Ref. 1 states that between 1989-1991, the gyroplane fatal accident rate in the U.K was 6 per 1000 flying hours, whereas the overall general aviation rate during 1990 was 0.015 per 1000 flying hours. As a consequence, there is heightened interest in this class of aircraft, and a new airworthiness and design standard (BCAR Section T) has been published by the U.K. Civil Aviation Authority, Ref. 2.

However, there is little substantive data at present to support the design standard, and the literature has not, until recently, addressed stability and control (Ref. 3). The objective of this Paper is therefore to contribute to a sparse literature on the subject of gyroplane flight mechanics, thereby directly supporting BCAR Section T. The specific aims of the work are: to explore the application, to the gyroplane, of previous research in rotorcraft system identification; to obtain robust estimates of longitudinal stability and control derivatives; and to use these derivatives to assess the nature of the flight dynamics of gyroplanes.

### **Background**

The gyroplane helped to pave the way for the development of the helicopter, introducing cyclic pitch control and blades attached to the rotor hub by means of a hinge. Unfortunately, with the one exception of Ref. 3, the literature has not hitherto addressed stability and control. The literature on gyroplanes nonetheless is considerable, Refs. 4-14 for example. However, in a contemporary context, this work is now primarily of historical significance. It provides the basis of the understanding of gyroplane flight, but does not address the issues of stability and control. Examination of the literature shows a logical development of the study of gyroplanes, from the elementary theory of gyroplane flight, to an analysis of aerodynamics and performance and ultimately rotor behaviour, but only for steady flight. Interest then apparently waned and the next logical stage in the study of the gyroplane i.e. stability and control, was not examined. For example, the work of Glauert includes the derivation of simple expressions for rotor speed as a function of loading and axial velocity, Ref. 4. Wheatley, Ref. 10 derived expressions for the flapping angles required for equilibrium flight, presenting results that show how coning, longitudinal and lateral flap angles vary with flight condition. Nowadays, these analyses would be recognisable as classical rotary-wing theory and analogous to that found in helicopter text books. Wheatley even examined higher harmonic components of blade flapping behaviour, Ref. 12.

It is in this context that gyroplane flight trials and the associated data analysis methods were planned. There is an extensive literature on system identification and parameter estimation, and application to the rotorcraft problem is well documented, e.g. Refs. 15-20. Tischler in particular has argued strongly in favour of the merits of frequency-domain identification, specifically directed towards the synthesis of non-parametric frequency responses. The repeatability and consistency achieved indicates that the frequency domain approach is robust.

The approach taken in this Paper is to adopt a frequency-domain equation-error method using linear

regression, to synthesise conventional 3 degree-of-freedom stability and control derivatives. This model structure is familiar to flight dynamicists, thereby facilitating general insight into fundamental behaviour of the gyroplane. Specific derivatives are directly related to individual, or group, effects that would otherwise be hidden in the aggregate presentation of a frequency response. The equation error method has limitations, as described in Refs. 15 and 18, although working in the frequency domain minimises some of the difficulties. The advantage is the simplicity of the approach, in concept and application. It is argued that good results can be obtained with a frequency-domain equation-error approach if careful design of the experiments, the equipment installation and execution of the flight trials is complemented by sound engineering judgement applied to the interpretation of the data.

### **Aircraft and Experimental Installation**

The aircraft used in this study was the VPM M16 gyroplane, Figure 1. It is of Italian origin, produced in kit form for assembly by the owner. The maximum all-up mass is 450 kg. The aircraft is powered by a four-cylinder two-stroke engine driving a three-bladed fixed pitch propeller. For helicopter engineers not familiar with gyroplanes, the rotor system is of an interesting configuration, typical of this class of aircraft. The two main rotor blades are bolted to a teeter bar, suspended from a teeter bolt. The blades are untwisted, and no cyclic pitch can be applied. This hub assembly is mounted on a spindle, about 200mm long, and this spindle pivots about its lower end to tilt the entire rotor fore and aft and laterally to effect pitch and roll control, respectively. In this regard, the aircraft could be classed as a tilt-rotor.

### **Figure 1: VPM M16 Gyroplane**

The experimental installation consisted of a digital on-board recording system, operating at 10 Hz. Anti-aliasing filters were incorporated. A nose-mounted air data probe containing sideslip and angle of attack vanes

was fitted, and an inertial unit measured angular velocities about three axes, and linear accelerations along these axes. A separate unit was used to measure roll and pitch angles. Pilot control positions were measured using potentiometers. Rotorspeed was also recorded. The front seat and flight controls were removed to accommodate the system. It was found that the aircraft's own indicated airspeed system suffered from a position error of about 8 mph across the speed range. All results are plotted with respect to the indicated airspeed, although the nose-mounted probe data was used for all analysis.

The identification of gyroplane dynamics presents a particular challenge, in addition to those normally met with helicopter system identification. The aircraft is light, which demands stringent limits on atmospheric conditions during the tests. Solo operation of this aircraft was essential due to the mass and space restrictions imposed by the instrumentation system. This placed particular demands on the test pilot's flying skills in order that the quality of the test inputs were not compromised.

### Data Analysis and Model Synthesis

The model structure for which coefficients are to be identified, is of conventional state-space form, i.e.

$$\dot{\underline{X}} = A\underline{X} + B\underline{u} \quad (1)$$

where

$$A = \begin{bmatrix} X_u & X_w & X_q & X_\theta & X_\Omega \\ Z_u & Z_w & Z_q & Z_\theta & Z_\Omega \\ M_u & M_w & M_q & M_\theta & M_\Omega \\ 0 & 0 & 1 & 0 & 0 \\ Q_u & Q_w & Q_q & Q_\theta & Q_\Omega \end{bmatrix}, \quad B = \begin{bmatrix} X_{\eta_s} \\ Z_{\eta_s} \\ M_{\eta_s} \\ 0 \\ Q_{\eta_s} \end{bmatrix} \quad (2)$$

and

$$\underline{x} = [u \quad w \quad q \quad \theta \quad \Omega]^T, \quad \underline{u} = [\eta_s] \quad (3)$$

This constitutes the longitudinal subset of the conventional 6 degree-of-freedom rigid-body flight mechanics model, with the important (and unique) addition of the rotorspeed degree of freedom. The rigid body states are taken to be with respect to a mutually orthogonal, right-handed frame of reference whose origin is at the centre of mass. The longitudinal and vertical axes are respectively parallel and normal to the keel of the aircraft.

The angular quantities in the state vector, and the control position, are all measured directly. The translational velocities  $u$  and  $w$  are obtained from airspeed, sideslip and angle of attack data measured at the nose-mounted boom, as follows.

$$\begin{aligned} u &= u_{probe} - q(z_{vane} - z_{cg}) + r(y_{vane} - y_{cg}) \\ w &= w_{probe} - p(y_{vane} - y_{cg}) + q(x_{vane} - x_{cg}) \end{aligned} \quad (4)$$

and

$$u_{probe} = \frac{V_f \cos \beta_{vane}}{\sqrt{1 + \tan^2 \alpha_{vane}}}; \quad w_{probe} = u_{probe} \tan \alpha_{probe} \quad (5)$$

The time histories of each variable were then converted into frequency domain information using a Discrete Fourier Transform, Ref. 20, given by

$$X(k\Delta f) = \Delta t \sum_{n=0}^{N-1} x_n e^{-i2\pi(kn)/N}; \quad k = 0, 1, 2, \dots, N-1 \quad (6)$$

which gives real and imaginary parts of  $X$ ,

$$\begin{aligned} \text{Re}[X(k\Delta f)] &= \Delta t \sum_{n=0}^{N-1} x_n \cos(2\pi(kn)/N); \\ \text{Im}[X(k\Delta f)] &= -\Delta t \sum_{n=0}^{N-1} x_n \sin(2\pi(kn)/N) \end{aligned} \quad (7)$$

The quality of these frequency domain data can be enhanced by standard processing techniques such as applying overlapped and tapered windows to the data, as recommended by Tischler, Ref. 20.

Each degree of freedom can then be treated separately, and formulation as a linear regression problem allows estimation of the coefficients. The state-space description is converted to the frequency domain, i.e.

$$i\omega \underline{x}(\omega) = A\underline{x}(\omega) + B\underline{u}(\omega) \quad (8)$$

Note that this assumes that any process noise is zero. The unknown coefficients of the  $A$  and  $B$  matrices are determined by solutions of the frequency domain equations

$$\begin{aligned} -\omega \text{Im}[\underline{x}(\omega)] &= A(\text{Re}[\underline{x}(\omega)]) + B(\text{Re}[\underline{u}(\omega)]) \\ \omega \text{Re}[\underline{x}(\omega)] &= A(\text{Im}[\underline{x}(\omega)]) + B(\text{Im}[\underline{u}(\omega)]) \end{aligned} \quad (9)$$

This solution applies equal weighting to real and imaginary part errors, which is consistent with the standard weighting for system identification on a Bode plot. The pitching moment equation for example, is then expressed as the two equations

$$\begin{aligned}
-\omega \operatorname{Im}[q(\omega)] &= M_u \operatorname{Re}[u(\omega)] + M_w \operatorname{Re}[w(\omega)] + \\
&M_q \operatorname{Re}[q(\omega)] + M_\theta \operatorname{Re}[\theta(\omega)] + \\
&M_\Omega \operatorname{Re}[\Omega(\omega)] + M_{\eta_s} \operatorname{Re}[\eta_s(\omega)] \\
\omega \operatorname{Re}[q(\omega)] &= M_u \operatorname{Im}[u(\omega)] + M_w \operatorname{Im}[w(\omega)] + \\
&M_q \operatorname{Im}[q(\omega)] + M_\theta \operatorname{Im}[\theta(\omega)] + \\
&M_\Omega \operatorname{Im}[\Omega(\omega)] + M_{\eta_s} \operatorname{Im}[\eta_s(\omega)]
\end{aligned} \tag{10}$$

The other degrees of freedom are in a similar form.

## Results

The test points were nominal airspeeds of 30, 50 and 70 mph. At each of these speeds, a doublet-type input was used to excite the short-term response, and the standard technique of displacing the stick to provoke a speed change before returning it to trim was used to excite any phugoid. Frequency sweep inputs were conducted only at the 70 mph test point. Figure 2 illustrates a typical frequency sweep. This type of test proved difficult to perform at 30 and 50 mph due to the ineffectiveness of the trim system on the aircraft at airspeeds less than 70 mph. The consequent out-of-trim stick force proved distracting and difficult to compensate for during the conduct of a sweep.

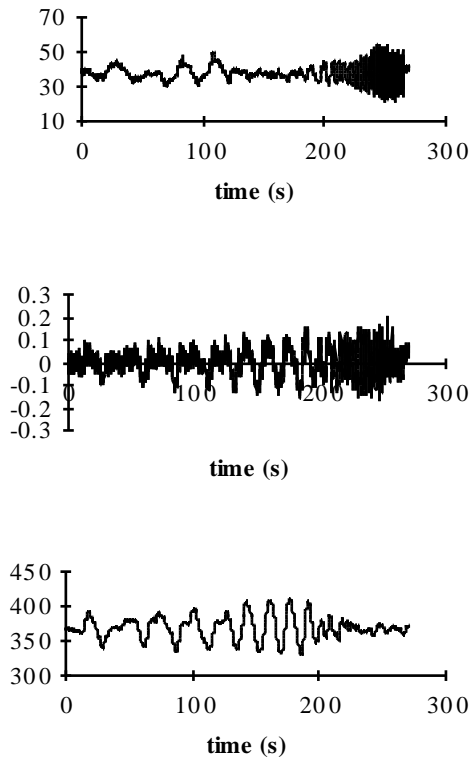


Figure 2: Response during frequency sweep test at 70 mph

An important aspect in any system identification study is the *identifiability* of the estimated parameters, Refs. 21, 22. This is particularly germane to the equation error approach. *Robust* estimates of the derivatives are those whose values can be judged to be invariant with the event, input type, estimation method or frequency range used, and for which a low standard error is calculated. *Verification* of the appropriateness of the identified model is usually achieved by confirming that it will predict the response to a dissimilar control input to that used in the identification. The issue of identifiability is particularly germane to the gyroplane problem as there is no literature on the vehicle's characteristics. These issues are explored next.

### Derivative estimates from dissimilar input types

Data from doublet and phugoid tests were zero-meaned and concatenated to provide a 90 second record length. The longitudinal derivatives estimated using these data are compared in Tables 1 to 4, with derivatives estimated from a frequency sweep. The standard error associated with each derivative is given in parentheses.

Consistent estimates of the derivatives are obtained, particularly in the pitching moment and rotor torque equations. The correlation coefficients are also in general good. The standard error associated with each estimate is relatively small, although for frequency

parameter	concatenated doublet/phugoid	frequency sweep
$R$	0.742	0.822
$X_u$	0.081 (0.056)	0.047 (0.025)
$X_w$	-0.126 (0.109)	-0.268 (0.058)
$X_q$	-3.976 (3.499)	-1.169 (1.380)
$X_\theta$	-9.036 (1.578)	-10.632 (0.851)
$X_\Omega$	-0.044 (0.013)	-0.025 (0.006)
$X_{\eta_s}$	0.010 (0.034)	-0.001 (0.013)

Table 1: X-force Derivative Comparisons

parameter	concatenated doublet/phugoid	frequency sweep
$R$	0.928	0.706

$Z_u$	-0.060 (0.025)	-0.128 (0.024)
$Z_w$	-0.788 (0.048)	-0.565 (0.057)
$Z_q$	23.665 (1.529)	26.446 (1.350)
$Z_\theta$	2.247 (0.690)	4.060 (0.832)
$Z_\Omega$	-0.054 (0.005)	-0.065 (0.006)
$Z_{\eta_s}$	-0.100 (0.015)	-0.098 (0.013)

**Table 2: Z-force Derivative Comparisons**

sweep-derived parameters the errors are generally smaller than with the concatenated doublet/phugoid. Although the force derivative estimates display less consistency than the pitching moment and rotor torque estimates, this is consistent with parameter estimation experience in general, where force derivatives have been more difficult to identify than moment derivatives. However, it is argued that these force derivative estimates are consistent to within the statistical error bounds associated with each derivative. The standard errors indicate that the corresponding derivatives will lie within the 95% confidence bounds associated with their respective estimates.

parameter	concatenated doublet/phugoid	frequency sweep
$R$	0.919	0.886
$M_u$	0.023 (0.003)	0.021 (0.001)
$M_w$	-0.065 (0.007)	-0.064 (0.003)
$M_q$	-1.213 (0.126)	-1.055 (0.076)
$M_\theta$	-0.449 (0.181)	-0.294 (0.047)
$M_\Omega$	-0.001 (0.0006)	-0.001 (0.0003)
$M_{\eta_s}$	0.029 (0.001)	0.028 (0.0007)

**Table 3: Pitching Moment Derivative Comparisons**

parameter	concatenated doublet/phugoid	frequency sweep
$R$	0.910	0.966
$Q_u$	1.373 (0.166)	1.378 (0.042)

$Q_w$	5.324 (0.628)	5.901 (0.126)
$Q_q$	12.590 (12.419)	7.679 (3.076)
$Q_\theta$	0 - fixed	0 - fixed
$Q_\Omega$	-0.129 (0.029)	-0.085 (0.007)
$Q_{\eta_s}$	0.305 (0.129)	0.314 (0.030)

**Table 4: Rotorspeed Derivative Comparisons**

Derivatives that physically ought to have negligible aerodynamic or propulsion force and moment contributions (i.e. those dominated by kinematic or gravitational terms), are  $X_\theta$  and  $Z_q$ . The former ought to have a value of approximately -9.81. Both input types give estimates of  $X_\theta$  and  $Z_q$  that are very similar, and in the case of  $Z_q$  also consistent with the mean flight speed of 28 m/s. This enhances confidence in the frequency sweep-derived Z-force derivatives, despite this equation providing the lowest correlation coefficient. Note that terms normally expected to be negligible or zero, such as  $Z_\theta$  and  $M_\theta$ , were retained in the regression as an additional check on model structure validity.  $Z_\theta$  is not negligible, although it is estimated with a relatively large standard error, and removing it from the regression proved to have little impact on the goodness of fit or the other parameters in the model. Removing  $M_\theta$  from the pitching moment model also had little effect on the other estimates, although it is estimated with a relatively low standard error, tending to suggest that it should be retained. However, its contribution to the overall pitch moment is approximately an order of magnitude smaller than the other terms in the equation, for the perturbations in  $\dot{x}$  and  $\dot{u}$  experienced in flight.

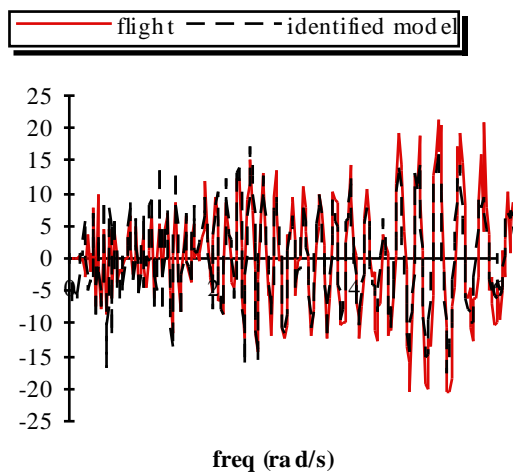
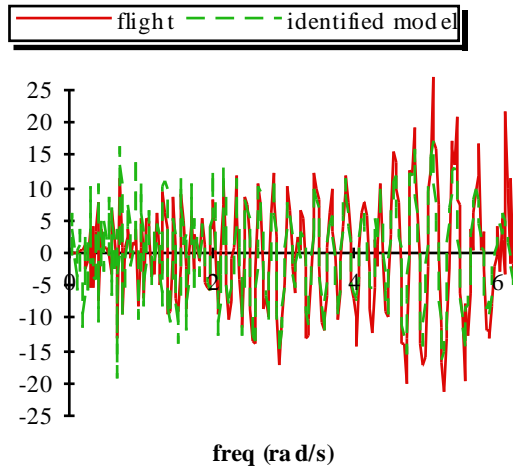


**Figure 3: Fit quality - flight and identified model pitching moment equation**

Estimates for the X-force derivative  $X_u$  are very small, with relatively large standard error. Indeed, the frequency sweep-derived value is positive. This parameter is the primary damping term in the phugoid mode, Ref. 23, and it would normally be expected to be substantially negative. As will be seen later in the Paper, inspection of the airspeed time histories suggests consistency with the identified values of  $X_u$ , in that there is little apparent damping of airspeed during the longer-term, phugoid-type oscillation.

The pitching moment derivatives  $M_u$ ,  $M_w$  and  $M_q$  describe an aircraft with classical longitudinal stability characteristics. Speed stability is positive ( $M_u > 0$ ), angle of attack stability is positive ( $M_w < 0$ ) and the primary pitch damping is positive ( $M_q < 0$ ). Figure 3 shows a comparison of the identified pitching moment equation's fit of the Fourier-transformed frequency sweep data. The fit is good across the frequency range used for the regression.

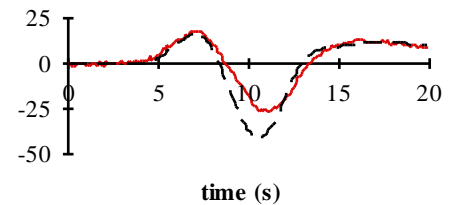
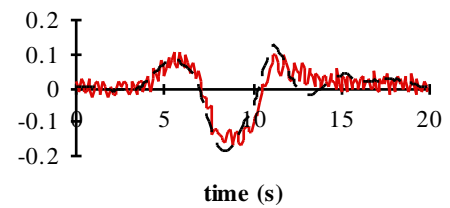
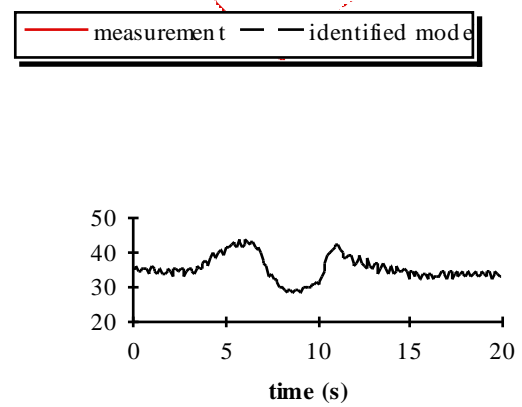


**Figure 4a : Identified model verification, 70 mph, short-term response**

### Verification

Figure 4a shows verification of a model identified from frequency sweep data. The model is driven by a doublet-type input made at the same nominal flight condition of 70 mph. The doublet-type input was used specifically to excite the short-term response, where the dominant variables were observed to be pitch rate and rotorspeed. The identified model provides a very good representation of the response, but displays a feature common to verification with other runs, in that any mismatch between identified model and measurement is associated with reduction in rotorspeed.

features of the response, giving added confidence that concatenated doublet/phugoid test inputs can be used for identification.

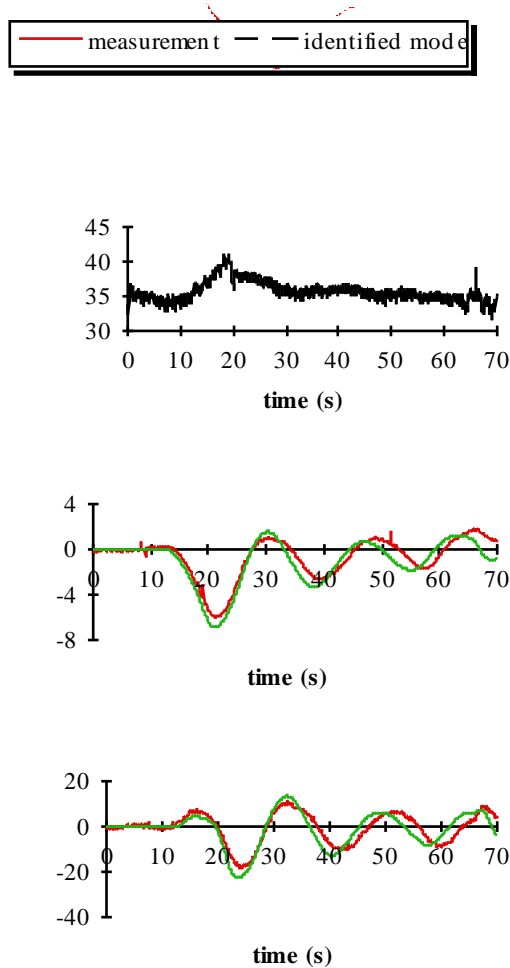


**Figure 4b : Identified model verification, 70 mph, phugoid response**

Figure 4b shows the model's ability to simulate measured behaviour during a phugoid test. Amplitude and phase of the  $u$  velocity and rotorspeed components of the phugoid mode are well represented by the identified model. The slight mismatch in the long-period response is the result of the model result being shifted in time by about 2 s relative to the measured response. This is perhaps not surprising for two reasons. First, the correlation coefficients shown previously indicate that the model structure may only approximate observed behaviour. Second, the input required for this test input produced a very substantial reduction in airspeed, which may take the identified model out of its limit of applicability. Notwithstanding this, the model does capture the substantial reduction in airspeed and rotorspeed before the control is returned to trim.

Unlike the 70 mph test point, the doublet-type input is sufficient to excite longer-term as well as short-term responses at 30 mph. This is shown in Figure 5 which also compares the response predicted by the identified model for 30 mph. This model captures the salient

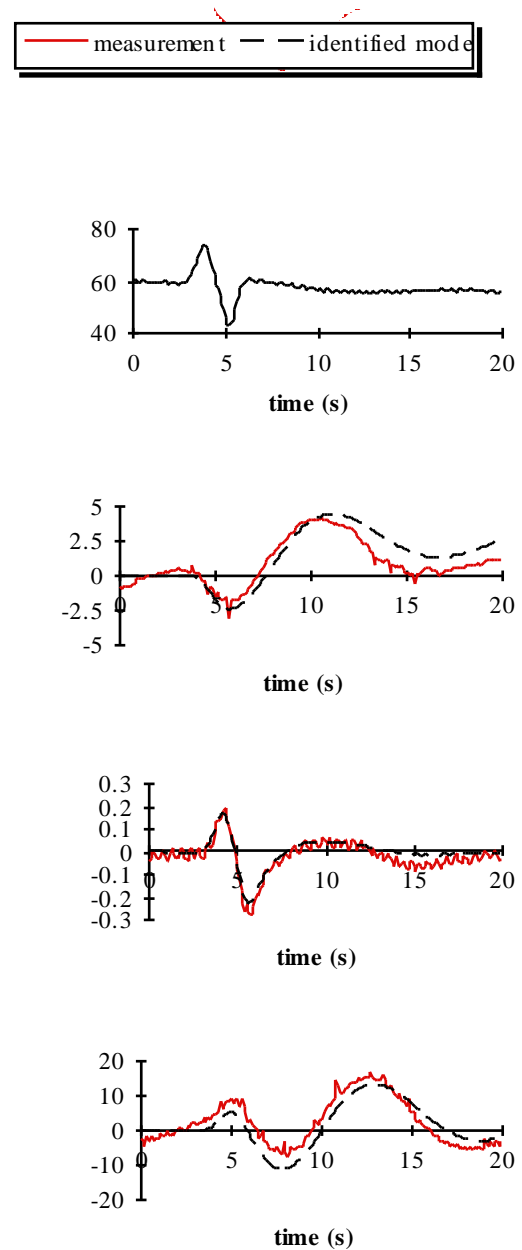


**Figure 5: Identified model verification, 30 mph**

### Assessment of Gyroplane Longitudinal Flight Dynamics

The foregoing provides a qualitative and quantitative basis for the judgement that the identified models provide a good representation of the longitudinal flight dynamics of the VPM M16 gyroplane. It is argued that they can therefore be used to assess the nature of the type's stability and controllability characteristics.

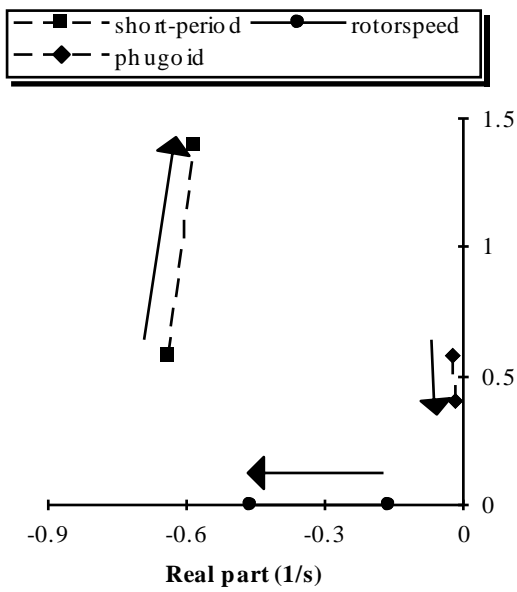


**Figure 6: Identified model eigenvalues, 30, 70 mph**

Figure 6 shows the eigenvalues of the synthesised models at 30 and 70 mph. The arrows indicate the progression from low to high speed. The two oscillatory modes are consistent with the frequency and damping of classical fixed-wing aircraft short-period and phugoid oscillations. The aperiodic mode is that of the rotorspeed degree of freedom. Assessment of the eigenvectors of the identified  $A$  matrices indicates that rotorspeed also features significantly in the rigid-body modes. The phugoid mode is relatively insensitive to changes in airspeed. The time to half amplitude is about 30-40 sec, its period 12-15 sec. The short-period mode is less than critically-damped throughout the speed range, with a damped natural frequency of between 0.1 and 0.25 Hz. The rotorspeed mode time to half amplitude lies between 1-4 sec.

Figure 7 presents the 95% confidence, 95% probability bounds of those identified derivatives that tend to determine fundamentally the dynamic characteristics. The relatively wide boundaries associated with  $X_u$ , and the small or even positive identified values are probably due to the fact that the propeller speed variations are not included in the model structure. The other derivative estimates all exhibit much narrower bounds. The aircraft exhibits "classical"

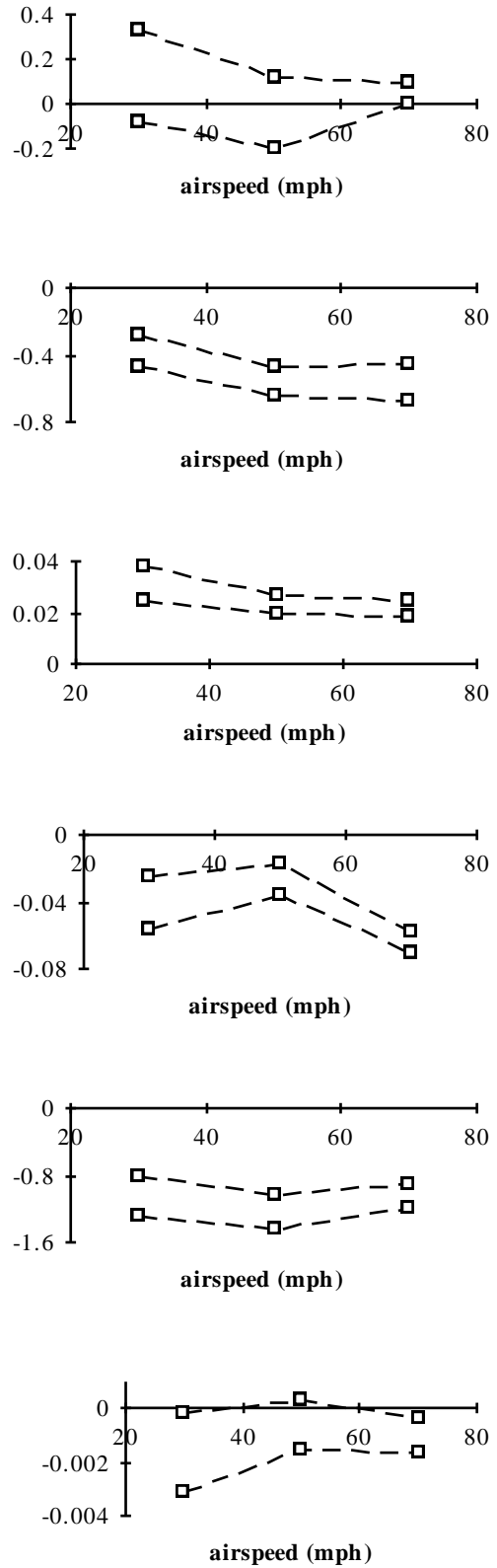


**Figure 7: Key identified force and pitching moment derivatives**

static stability characteristics ( $M_u > 0$ ,  $M_w < 0$ ,  $M_q < 0$ ) across the speed range, and not just at 70 mph as noted previously. The derivative unique to the gyroplane is  $M_\Omega$ , and being negative, will *tend* to be stabilising. This is because an increase in rotorspeed will result in a nose-down moment, tending to reduce the axial flow through the rotor, and hence tending to reduce the original rotorspeed disturbance.

$M_u$  is an indication of the speed stability of the aircraft, and the exhibited trend is consistent with the measured longitudinal stick position in trimmed flight. Unmodelled propeller speed and hence thrust variations may very well have a role to play in this derivative, quite apart from the usual rotor and tailplane contributions.  $M_w$  is the angle of attack stability, and unusually for a rotorcraft, is negative throughout the speed range. This is an important derivative as it holds the clue to a general understanding of gyroplane flight dynamics. Unaugmented rotorcraft generally rely on a horizontal tailplane to provide  $M_w < 0$ . This is because the natural tendency of the rotor (and hence thrust vector) is to flap back with angle of attack, or  $w$  disturbances. Since rotor thrust also increases with  $w$ , and the thrust line usually passes close to the centre-of-mass in undisturbed flight, then both effects sum to produce  $M_w > 0$ , Ref. 24. However, the profile of  $M_u$  and  $M_q$  with speed would tend to suggest that the tailplane on this gyroplane is somewhat ineffective, despite its relatively large size. This is consistent with wind tunnel tests on this configuration, Ref. 25. Pusher propeller configurations will tend to produce a stabilising contribution to  $M_w$  as a consequence of the propeller normal force increasing with angle of attack disturbances. However, the relatively low power of the engine would suggest that this effect is small, and if considered with the very unclean aerodynamic environment in which the propeller operates, renders this phenomenon difficult to quantify.

Ref. 3 postulated that gyroplane longitudinal stability could be dominated by the vertical position of the centre-of-mass relative to the propeller thrust line, and a configuration with propeller thrust line below the centre-of-mass could exhibit  $M_w < 0$  even at low airspeeds where any tailplane contribution would be negligible. The mechanism for this is shown in Figure 8. The nose-up moment produced by a configuration with propeller thrust line below the centre-of-mass will require to be trimmed in equilibrium flight by having the main rotor thrust line passing behind the centre of mass as shown. In disturbed flight then, the possibility exists of the reduction in nose-down moment caused by the rotor flapping back, being overcome by the contribution from the increase in thrust, resulting in  $M_w < 0$ . Note that the result  $M_\Omega < 0$  identified here is also consistent with such a configuration. Calculations based on mass and balance measurements do place the vertical position

of the centre of mass 0.02 m above a line passing through the centre of the propeller hub.

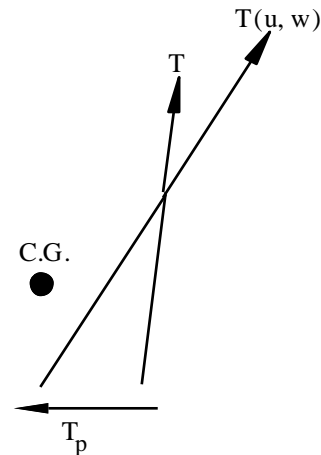


**Figure 8: Rotor and Propeller Forces in Equilibrium and Disturbed Flight**

Further validation of this postulate comes from the marked reduction in  $M_w$  (and  $M_\Omega$ ) at 50 mph. This is close to the minimum drag speed, and hence where the propeller thrust would be a minimum also. Any pitching moment from the propeller would therefore be a minimum, and the main rotor thrust line would be at its closest to the centre of mass in equilibrium flight, i.e. tending to give a smaller  $M_w$  than at the higher-power speeds of 30 and 70 mph.

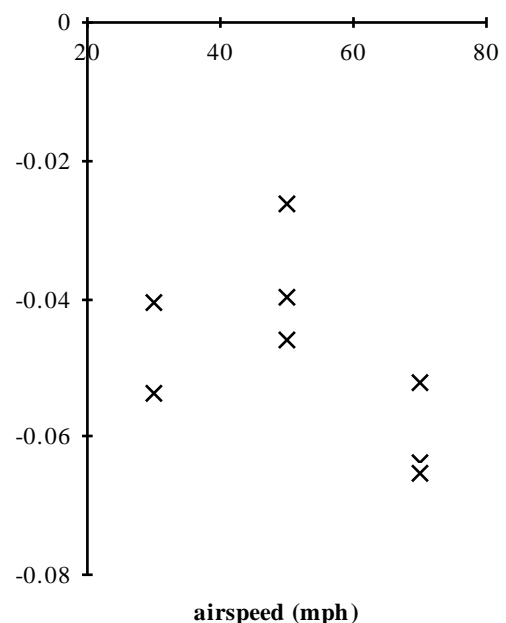


**Figure 9: Multi-run consistency of result in  $M_w$**

Figure 9 shows three estimates for  $M_w$  at each speed, obtained from different flights. The multi-run

consistency exhibited serves to confirm  $M_w < 0$  throughout the speed range, even at low speed, and also the observed effect that  $M_w$  is reduced in magnitude at around the minimum drag speed.

Figure 10 shows the identified derivatives in the rotor torque equation. It is impossible to relate these to any previous quantitative work. However, qualitatively  $Q_u$  and  $Q_w$  are consistent with Glauert's seminal work, Ref. 4 in that an increase in airspeed and axial velocity will both tend to increase rotorspeed ( $Q_u > 0$ ,  $Q_w > 0$ ). Although the primary damping term  $Q_\Omega$  decreases with airspeed, the rotorspeed mode itself exhibits the opposite trend, Figure 6. This indicates the extent of inter-modal coupling between the rotorspeed and body degrees of freedom. Finally, the control derivative  $T_{\eta_s}$  shows that the rotorspeed response will become increasingly sensitive to control application with airspeed.

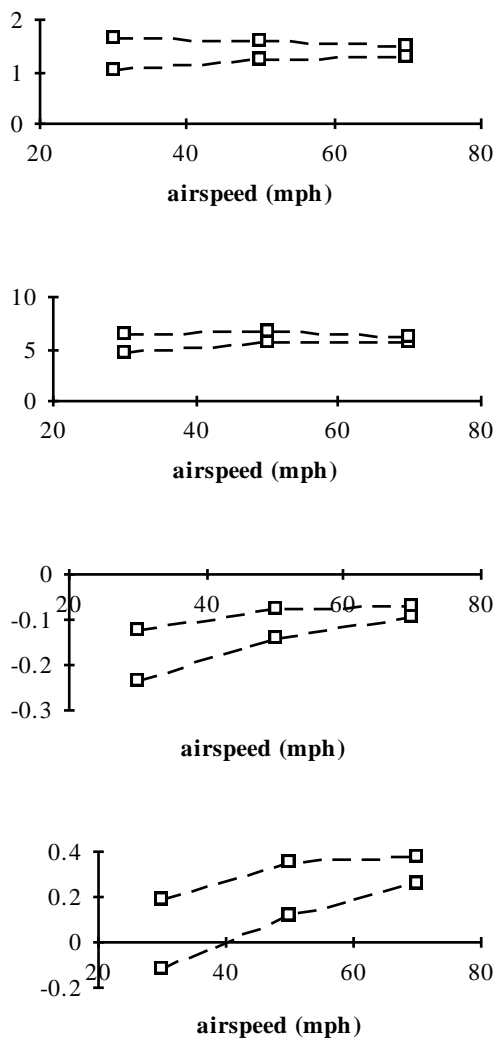


Figure 10: Rotor torque derivatives

## Discussion

These results are significant for several reasons. First, they are unique in that the literature indicates that no previous in-flight investigation of gyroplane stability and control has taken place. Second, the results are timely in that the U.K. gyroplane accident record is poor, and a substantial number of fatal accidents remain largely unexplained. In addition, the U.K.'s new airworthiness and design standard BCAR Section T is a unique code, and requires substantive data, having been developed largely from other codes. Third, contemporary flight test and data analysis techniques have been used, which helps to consolidate the status of system identification and parameter estimation for rotorcraft. The gyroplane joins conventional single main and tail rotor helicopters, tandem rotor helicopters and tilt-rotors as rotorcraft that have enjoyed the successful application of these tools to a real engineering problem.

Although the results obtained are specific to the VPM M16 gyroplane, they are of more general significance for two reasons. First, as gyroplane stability and control has not featured in the literature until recently, cataloguing the characteristics of one type benchmarks the quantification of gyroplane stability in general. Second, the result in  $M_w$  in particular, can be rationalised in terms of centre of mass position with respect to propeller thrust line, an issue of direct relevance to all gyroplanes. The results can also be applied directly to the development of the airworthiness and design standard BCAR Section T, as they constitute the only documentation of actual aircraft characteristics to date. For example, there is no requirement for balance to be specified in terms of vertical centre-of-mass position in relation to the propeller thrust line. The results suggest that this is an important consideration in conferring positive angle of attack stability  $M_w$ , which it is relatively easy to show has a key role to play in stabilising the phugoid mode of rotorcraft, Ref. 23.

Finally, the results quantify the extent to which the rotorspeed degree of freedom is significant in gyroplane flight mechanics. The pilot relies on management of flight state to maintain rotorspeed, having no direct control over it. Although the results indicate that the rotorspeed mode is stable, it is closely coupled with the conventional rigid body degrees of freedom. The rotor torque derivatives indicate that rotorspeed is sensitive to airspeed and angle of attack perturbations and this may have implications for handling in marginal situations.

## Future Developments

The development of rotorcraft flight dynamics models forms a major and important area of research within the Aerospace Department at the University of

Glasgow. Naturally there is a requirement for high quality flight test data for validation purposes. The experience gained in undertaking gyroplane flight trials for the CAA has given the Department confidence in their ability to conduct such experiments independently. Consequently a 2-seat Montgomerie Gyroplane was purchased with the aim of instrumenting this vehicle for flight trials. The vehicle, shown in Figure 11 was purpose built for flight trials with the rear seat removed to provide space for an instrument pallet and on-board computer. An improved electrical system was also added to ensure appropriate voltages and power supply for the sensors. Table 5 gives some basic configurational parameters for the Montgomerie aircraft in comparison with the VPM M16.

**Figure 11: University of Glasgow Research Gyroplane**

Parameter	VPM M16	Montgomerie
Max T.O. Mass	426kg	385kg
Rotor Diameter	8.3m	7.62m
Powerplant	120hp Arrow	75hp Rotax 618
Blade Type	VPM	McCutcheon
Max Level Spd	70mph	85mph

**Table 5: Comparison of Basic Parameters for 2 Gyroplanes**

Lessons learned in the CAA trials have been put into practise in the design of the sensor and data acquisition packages for the in-house aircraft. Data acquisition is by a Kontorn Elektronik industrial PC recording 64 channels at a sample rate of 64Hz using a National Instruments DAQ card and Labview software, telemetry being possible via a radio modem link. Initial trials will focus on recording standard flight dynamics data and hence the sensor package consists of:

- i) one British Aerospace Systems and Equipment three axis accelerometer to measure the component inertial accelerations,
- ii) three British Aerospace Systems and Equipment rate gyros to measure the attitude rates,
- iii) three British Aerospace Systems and Equipment angle indicators to measure attitude angles,

- iv) one Space Age Technology mini air data boom to measure airspeed, angle of attack and angle of sideslip,
- v) four Space Age Technology displacement transducers to measure the pilot's control inputs (fore and aft stick, pedals and throttle).

The aircraft is equipped with a Garmin GPS receiver, the data from which will also be downloaded to the on-board computer. It is proposed to conduct a baseline set of flight trials to ascertain the basic performance, and stability and control characteristics of the aircraft during the summer of 1998. Subsequent trials will be performed to support the current rotorcraft research in the Department, for example strain gauges and pressure transducers will be fitted to the blades to validate current modelling projects in the areas of wake dynamics and blade aeroelasticity.

### Conclusions

Robust identification of gyroplane longitudinal stability and control derivatives has been possible using relatively straightforward frequency-domain parameter estimation tools.

Unusually for rotorcraft in general, the type examined displays "classical" longitudinal dynamic stability characteristics, and is stable throughout the speed range. However, rotor speed is an important variable and is closely coupled with the conventional rigid-body degrees of freedom.

Interpretation of the identified stability derivatives indicates that the vertical position of the centre of mass in relation to the propeller thrust line may have an important role to play in gyroplane longitudinal stability.

The results contribute directly to the development of the UK gyroplane airworthiness and design standard, BCAR Section T in the important areas of dynamic stability, and weight and balance.

### Acknowledgement

This work was conducted for the U.K. Civil Aviation Authority under Research Contract No. 7D/S/1125. The Technical Authority was Mr. David Howson.

### References

1. Anon, "Airworthiness Review of Air Command Gyroplanes", Air Accidents Investigation Branch Report, Sept. 1991.
2. Anon, "British Civil Airworthiness Requirements, Section T, Light Gyroplane Design Requirements"

- Civil Aviation Authority Paper No. T 860 Issue 2, Jul. 1993.
3. Houston, S. S., "Longitudinal Stability of Gyroplanes", *The Aeronautical Journal*, Vol. 100, No.991, 1996, pp. 1-6.
  4. Glauert, H., "A General Theory of the Autogyro", *Aeronautical Research Committee Reports and Memoranda No. 1111*, Nov. 1926.
  5. Lock, C. N. H., "Further Development of Autogyro Theory Parts I and II", *Aeronautical Research Committee Reports and Memoranda No. 1127*, Mar. 1927.
  6. Glauert, H., "Lift and Torque of an Autogyro on the Ground", *Aeronautical Research Committee Reports and Memoranda No. 1131*, Jul. 1927.
  7. Lock, C. N. H., Townend, H. C. H., "Wind Tunnel Experiments on a Model Autogyro at Small Angles of Incidence", *Aeronautical Research Committee Reports and Memoranda No. 1154*, Mar. 1927.
  8. Glauert, H., Lock, C. N. H., "A Summary of the Experimental and Theoretical Investigations of the Characteristics of an Autogyro", *Aeronautical Research Committee Reports and Memoranda No. 1162*, Apr. 1928.
  9. Wheatley, J. B., "Wing Pressure Distribution and Rotor-Blade Motion of an Autogyro as Determined in Flight", *NACA TR 475*, 1933.
  10. Wheatley, J. B., "An Aerodynamic Analysis of the Autogyro Rotor with a Comparison Between Calculated and Experimental Results", *NACA TR 487*, 1934.
  11. Wheatley, J. B., Hood, M. J., "Full-Scale Wind-Tunnel Tests of a PCA-2 Autogyro Rotor", *NACA TR 515*, 1935.
  12. Wheatley, J. B., "An Analytical and Experimental Study of the Effect of Periodic Blade Twist on the Thrust, Torque and Flapping Motion of an Autogyro Rotor", *NACA TR 591*, 1937.
  13. Schad, J. L., "Small Autogyro Performance", *Journal of the American Helicopter Society*, Vol.10, No. 3, 1965, pp. 39-43.
  14. McKillip, R. M., Chih, M. H., "Instrumented Blade Experiments Using a Light Autogyro", *Proceedings of the 16th. European Rotorcraft Forum*, Glasgow, Scotland, Sept. 1990.
  15. Fu, K.-H., Marchand, M., "Helicopter System Identification in the Frequency Domain", *Proceedings of the 9th. European Rotorcraft Forum*, Stresa, Italy, Sept. 1983.
  16. Tischler, M. B., et al, "Demonstration of Frequency-Sweep Testing Technique using a Bell 214-ST Helicopter", *NASA TM-89422*, April 1987.
  17. Tischler, M. B., "Frequency-Response Identification of XV-15 Tilt-Rotor Aircraft Dynamics", *NASA TM-89428*, May 1987.
  18. de Leeuw, J. H., "Identification Techniques, Model Structure and Time Domain Methods", *AGARD LS178*, pp. 5-1 to 5-9, October 1991.
  19. Kaletka, J., "Instrumentation and Data Processing", *AGARD LS178*, pp. 3-1 to 3-18, October 1991.
  20. Tischler, M. B., "Identification Techniques, Frequency Domain Methods", *AGARD LS178*, pp. 6-1 to 6-4, October 1991.
  21. Houston, S. S., Black, C. G., "On the Identifiability of Helicopter Models Incorporating Higher Order Dynamics", *AIAA Journal of Guidance, Control and Dynamics*, Vol. 14, No. 4, July-August 1991, pp. 840-847.
  22. Murray-Smith, D. J., "Modelling Aspects and Robustness Issues in Rotorcraft System Identification", *AGARD LS178*, pp. 6-1 to 6-4, October 1991.
  23. Padfield, G. D., "On the Use of Approximate Models in Helicopter Flight Mechanics", *Vertica*, Vol. 5, No. 3, 1981, pp. 243-259.
  24. Bramwell, A. R. S., "Helicopter Dynamics", *Arnold*, London, 1976, pp. 199-200.
  25. Coton, F., et. al., "Wind Tunnel Testing of a 1/3rd. Scale Model Gyroplane", *Proceedings of the 9th. European Rotorcraft Forum*, Sept. 1983.